High-pressure transition to the post-barite phase in BaCrO_{4} hashemite

D. Santamaría-Pérez, Ravhi S. Kumar, A. J. Dos santos-García, D. Errandonea, R. Chuliá-Jordán, R. Saez-Puche, P. Rodríguez-Hernández, and A. Muñoz

Phys. Rev. B **86**, 094116 — Published 28 September 2012

DOI: 10.1103/PhysRevB.86.094116

High-pressure transition to the post-barite phase in BaCrO4 Hashemite.

D. Santamaría-Pérez[1,†,*], R.S. Kumar[2], A.J. Dos Santos-García[3], D. Errandonea[4,†], R. Chuliá-Jordán[1], R. Saez-Puche[3], P. Rodríguez-Hernández[5,†], A. Muñoz[5,†]

[1] *Departamento de Química Física I, Universidad Complutense de Madrid, Avenida Complutense s/n, 28040 Madrid, Spain*
[2] *High Pressure Science and Engineering Center, Department of Physics and Astronomy, University of Nevada–Las Vegas, 4505 Maryland Parkway, Las Vegas, Nevada 89154-4002, USA*
[3] *Departamento de Química Inorgánica, Universidad Complutense de Madrid, Avenida Complutense s/n, 28040 Madrid, Spain*
[4] *Fundación General de la Universitat de València, Edificio de Investigación, C. Dr. Moliner, 50, Burjassot, 46100 Valencia, Spain*
[5] *Departamento de Física Fundamental II, Universidad de La Laguna, La Laguna, Tenerife, Spain*

† *MALTA Consolider Team*

Abstract

A recent high-pressure study on barium chromate $BaCrO_4$ reported a phase transition but the structure of the high-pressure phase structure could not be identified. This high-pressure phase was suggested to have a monoclinic structure different from other high-pressure forms of ABO_4-type compounds. In this work, we have carried out x-ray diffraction measurements up to 46 GPa using He as quasi-hydrostatic pressure medium and Density-Functional Theory calculations. Our studies allow us identifying the high-pressure phase as the $P2_12_12_1$ post-barite-type phase, recently reported for $BaSO_4$. The equations of state of both, the low- and the high-pressure phases have been determined. Elastic constants of the initial barite-type phase were calculated and the shear and Young moduli, and the Poisson coefficient deduced from them. Finally Raman and infrared active modes are also calculated, discussed, and compared with experiments when possible. As a first approximation, the vibrations can be separated in internal vibrations of the CrO_4 tetrahedra and vibrations where the tetrahedral units behave as rigid units. Pressure coefficients of the different modes are reported being two soft modes found for the HP phase.

Introduction

Minerals of the barite-type family are of great interest for Earth[1] and material sciences[2-4]. This family includes some $A^{II}B^{VI}O_4$ sulphates, chromates, phosphates and perclorates, amongst others, which crystallize in an orthorhombic structure (space group (S.G.): *Pnma*). Its structure has been usually described in terms of oxygen polyhedra, the oxide being formed by isolated [BO_4] tetrahedra and complex [AO_{12}] dodecahedra, but a more recent description in terms of its *AB* cation subarray provides a different point of view, showing the similarity between the *AB* sublattice in the ternary oxide and the structure of the FeB alloy (see Fig. 1a). A more detailed analysis of this structure type can be found in Refs. [5-7]. Many ternary halides adopt this structure as well.

On the other hand, compounds adopting this type of structure have been of renewed interest regarding their high-pressure (HP) behaviour[6, 8-11]. Although experimental evidences of post-barite transitions are known since the pioneering work of Bridgman[12], the structural determination of the post-barite phase could not be achieved until the last year. Santamaría-Pérez *et al*. found that barite transforms into another orthorhombic structure (S.G. $P2_12_12_1$, Fig. 1b), with no change in the coordination number of *A* or *B* atoms ([BO_4] tetrahedra and [AO_{12}] dodecahedra)[11]. However, the second coordination sphere of the *A*/*B* atoms presents an increase of neighbouring atoms from 7 to 8; *i.e*. the cation subarray *AB* of the post-barite structure can be considered as an intermediate framework between the FeB-type (corresponding to the initial *Pnma* barite structure) and the CsCl-type structures[6]. Adittionally, Errandonea and coworkers have recently proposed a monoclinic $P2_1/m$ structure for a HP post-barite phase in $AgClO_4$, which also presents an *AB* sublattice closely related to the CsCl-type structure[13].

The determination of the post-barite phase has allowed completing the lower right quadrant of the Bastide diagram which, based on the relative cation sizes, provides systematic trends in phase transitions in ABO_4 isotypes[14]. Thus, the north-east phase-transition rule predicts that compounds with the monazite-type structure would transform upon compression either to the scheelite or the barite structure. For instance, the latter behaviour was observed in the phosphate $LaPO_4$[15] and in the sulphate $CaSO_4$ at high pressures[16, 17]. Therefore, post-barite could be a potential structure for both the monazite- and the barite-type structures at high pressures.

Thus, intrigued by the recent report of a high-pressure phase transition in the barite-type $BaCrO_4$ compound (mineral name: Hashemite) at about 10 GPa, where no

structural determination could be done[9], we have reinvestigated the high-pressure behaviour of barium chromate by means of angle-dispersive X-ray diffraction (ADXRD) measurements using He as pressure medium. The experiments allow identifying the orthorhombic post-barite phase previously found in $BaSO_4$ under compression. Our results are supported by total-energy *ab initio* calculations.

Experimental and theoretical methods

Experimental details

Polycrystalline $BaCrO_4$ powder was prepared via the traditional solid state reaction. Pre-dried stoichiometric amounts of Cr_2O_3 and $BaCO_3$ (>99%, Aldrich) were intimate grinded in acetone and then fired 850°C for 16 hours. The resulting powder was ground again and pressed uniaxially into pellets at 1 metric ton. The pellets were then fired at 950°C for 36 hours. The X-ray diffraction pattern at ambient pressure (AP) confirmed the barite-type structure.

High-pressure ADXRD experiments were carried out up to 46 GPa at 16-IDB beamline of the HPCAT at the Advanced Photon Source (APS). We used an incident monochromatic wavelength of 0.37379 Å focused down to 10 μm × 10 μm. Measurements were performed in a symmetric diamond-anvil cell (DAC) with diamond culets of 300 μm and a drilled rhenium gasket (100-μm diameter hole). The diffraction patterns were recorded on a MAR345 image plate located at 350 mm from the sample. Barium chromate powder was loaded in the diamond-anvil cell using helium (He) as pressure-transmitting medium to guarantee quasi-hydrostatic conditions in almost the whole pressure range covered by the experiments. Detector calibration, correction of distortion and integration to conventional 2θ-intensity data were carried out with the Fit2D software[18]. In this study the pressure was determined using the ruby fluorescence technique[19]. The indexing and refinement of the powder patterns were performed using the FULLPROF[20] and POWDERCELL[21] program packages.

Calculation details

We have performed *ab initio* total-energy calculations within the density functional theory (DFT)[22] using the plane-wave method and the pseudopotential theory with the

Vienna *ab initio* simulation package (VASP)[23-26]. We have used the projector-augmented wave scheme (PAW)[27, 28] implemented in this package to take into account the full nodal character of the all-electron charge density in the core region. Basis set including plane waves up to an energy cutoff of 520 eV were used in order to achieve highly converged results and accurate description of the electronic properties. The description of the exchange-correlation energy was performed with the generalized gradient approximation (GGA) with the PBEsol prescription[29]. A dense special k-points sampling for the Brillouin Zone (BZ) integration was performed in order to obtain very well converged energies and forces. At each selected volume, the structures were fully relaxed to their equilibrium configuration through the calculation of the forces and the stress tensor. In the relaxed equilibrium configuration, the forces on the atoms are less than 0.006 eV/Å and the deviation of the stress tensor from a diagonal hydrostatic form is less than 1 kbar (0.1 GPa). From our results we obtain the E-V 3rd-order Birch-Murnaghan equation of state (EOS) that can be fitted using a standard fitting procedure in order to obtain the bulk modulus and its pressure derivative. We also obtain the relative stability of the different analysed structures. Our study is a T= 0 K (zero point effects are not included). A phase transition occurs in our study when two phases have the same entalphy ($E_1 + P_t \cdot V_1 = E_2 + P_t \cdot V_2$). This allows us to obtain the theoretical transition pressure under these conditions. The application of DFT-based total-energy calculations to the study of semiconductors properties under high pressure has been reviewed in Ref. [30], showing that the phase stability, electronic and dynamical properties of compounds under pressure are well described by DFT.

We have also performed lattice dynamics calculations of the phonons at the zone center (Γ point) of the BZ. Our theoretical results enable us to assign the Raman modes observed for the different phases. Furthermore, the calculations provide information about the symmetry of the modes and polarization vectors. Highly converged results on forces are required for the calculation of the dynamical matrix. We use the direct force constant approach (or supercell method)[31]. The construction of the dynamical matrix at the Γ point of the BZ is particularly simple and involves separate calculations of the forces in which a fixed displacement from the equilibrium configuration of the atoms within the *primitive* unit cell is considered. Symmetry aids by reducing the number of such independent displacements, reducing the computational effort in the study of the analyzed structures considered in this work. Diagonalization of the dynamical matrix provides both the frequencies of the normal modes and their polarization vectors. This

allows us to identify the irreducible representation and the character of the phonons modes at the Γ point.

Mechanical stability of homogeneous crystals is an interesting subject that can provide important information concerning the study of the structural transformations via the stability criteria related with the mechanical properties. Knowledge of the elastic behavior can be essential for many practical applications. These elastic constants can be obtained computing the macroscopic stress after the application of a small strain by using the stress theorem[32]. Alternatively, it can be also calculated using density functional perturbation theory (DFPT)[33]. For the evaluation of the elastic constants, first we obtain the ground state relaxed structure, and latter the structure was strained in different directions according to their symmetry in order to obtain the elastic constants. The total-energy variations were evaluated according to a Taylor expansion[34] for the total energy with respect to the applied strain. Due to this fact it is important to check that the strain used in the calculations guarantees the harmonic behavior. This allows us to obtain the C_{ij} elastic constants in the Voigt notation and the number of independent elastic constants is reduced completely by crystalline symmetry[35].

Results and discussion

Figure 2 shows a selection of our ADXRD data for $BaCrO_4$ collected at several selected pressures with He as pressure medium. It is necessary to point out that the crystal sizes of our powdered sample are not uniform and, consequently, some texturing effects appear in the X-ray diffraction patterns. This unwanted effect entails that the relative intensities of the diffraction maxima are not accurate, affecting the quality of structural refinements. At ambient conditions, the X-ray diffraction pattern corresponds to the orthorhombic barite-type structure previously reported (S.G. *Pnma*)[36, 37] with similar lattice parameters: a = 9.1165(6) Å, b = 5.5264(4) and c = 7.3347(5) Å [V = 369.5(1) $Å^3$] (see Table I). The high-pressure XRD patterns could be indexed in the initial *Pnma* phase up to 13.6 GPa. Upon further compression additional diffraction peaks appear (arrows in the diffraction patterns at 16.6 GPa), what indicates the onset of a phase transition in $BaCrO_4$. In parallel, the intensity of the peaks of the low pressure phase gradually decreases. This transition pressure is considerably higher than the 9.8 GPa reported by Huang *et al*. using a 4:1 methanol-ethanol mixture as pressure transmitting medium[9]. Thus, the lack of hydrostaticity drives the onset of the phase

transition to occur at lower pressures, as it has also been observed in other compounds[38, 39], in particular in isomorphic $BaSO_4$[11].

The variation of the volume (Fig. 3a) and lattice parameters (Fig. 3b) of the initial phase with pressure was obtained from the present data. The pressure-volume curves were analyzed using a third-order Birch-Murnaghan equation of state (EOS). By fixing the zero-pressure volume (V_0) to its measured value, we obtained the bulk modulus (B_0) and its pressure derivative (B'_0), which are collected in Table II. The experimental values of these characteristic parameters are also in good agreement with those obtained from *ab-initio* calculations (see Table II). As can be seen in Fig. 3b, the contraction of the lattice parameters is rather anisotropic. For instance, according to our experiments, the relative contractions for *a*, *b* and *c* between room pressure and 16.6 GPa are 4.33, 6.96 and 7.29%, respectively. These values are also in good agreement with those from theoretical simulations, where *a*, *b* and *c* axes decrease 4.01, 7.2 and 7.52%, respectively, in this pressure range. Additionally, the evolution of the different axes can be described by a second-order polynomial function: $a(\text{Å}) = 9.114(5) - 0.036(2)\cdot P + 7.5(9)\cdot 10^{-4}\cdot P^2$, $b(\text{Å}) = 5.517(7) - 0.041(2)\cdot P + 11(1)\cdot 10^{-4}\cdot P^2$ and $c(\text{Å}) = 7.333(5) - 0.044(2)\cdot P + 7.0(8)\cdot 10^{-4}\cdot P^2$, where the pressure *P* is in GPa. Results are in good agreement with Huang's data[9] below 7.2 GPa but, at higher pressures, our data shows a slightly larger compressibility of the lattice parameters (see Figures 3a and 3b). This fact entails that the B'_0 value obtained by Huang *et al*. is considerably large ($B'_{0,\,\text{Huang}} = 6.8$), which evidences the existence of non-hydrostatic effects above this pressure. Note also that the compressibility of barium chromate is slightly higher than that of barite itself ($BaSO_4$), where the bulk modulus and its first pressure derivative are $B_0 = 58.6$ GPa and $B_0' = 4.8$.

From this observation, assuming that the [BaO_{12}] polyhedra are equally compressible in both compounds, it can be inferred that the volume of the [CrO_4] tetrahedral units decrease more rapidly with pressure than that of the [SO_4] units. Furthermore, the compressibility of the $ACrO_4$ structures is intimately related with that of the *A*-centered oxygen polyhedra. In other words, the *A* – O bonds are usually by far the most compressible. The bulk moduli of chromates with divalent *A* cations seem to depend on both, the average *A* – O distance (d) in this polyhedra and the coordination number of the *A* atom (CN_A). Thus, the experiential criterion, $B_0(\text{GPa}) = 286(16) - 109(8)\cdot d^3/CN_A$ would explain the bulk moduli of the barite-type $BaCrO_4$ (54 GPa), the monazite-type $PbCrO_4$ (57 GPa)[40] and the zircon-type $CaCrO_4$ (104 GPa)[41] structures.

Additional measurements of the bulk moduli of chromates are necessary to validate such relationship.

Above 16.6 GPa, the XRD patterns could be indexed using two different phases:

(i) A *Pnma* barite-type structure, similar to the initial structure, except for the sudden small change in the *b* and *c* lattice parameters at this pressure. The *b* axis contracts approximately 3.3%, the *c* axis expands approximately 0.6%, and the *a* axis remains nearly constant between 16.6 and 19.6 GPa, with the volume decreasing in a continuous way (see Figs. 3a and 3b).

(ii) A different orthorhombic structure whose structural model could correspond to the HP phase found in barite[11], S.G. $P2_12_12_1$. This post-barite phase was also recently found in $CeVO_4$ under compression[42]. The indexation of this high-pressure phase could be only performed above 27.4 GPa using 10 diffraction lines that were not explained by the barite-type phase (see in inset of Fig. 4 the limited quality of the data above 30 GPa). Attempts to index the lines of the diagrams upon compression between 16.6 GPa and 27.4 GPa were unsuccessful, suggesting that the extra peaks in fact correspond to one or several polymorphs with intermediate structures. We have also examined the monazite-type, the $AgMnO_4$-type and the monoclinic $P2_1/m$ unit cell proposed by Huang and coworkers[9], but their diffraction peak positions failed to match the HP phase.

The slowness of the phase transition to the $P2_12_12_1$ post-barite structure becomes apparent in the wide pressure range of phase coexistence. The LeBail fit of the XRD pattern at 45.9 GPa depicted in Figure 4 illustrates the quality of the indexation. It is also important to remark that, despite the texturing effects of the XRD patterns, the relative intensity of the Bragg peaks of the high-pressure phase is not far from that predicted for the $P2_12_12_1$ post-barite structural model. A tentative estimation of the relative fraction of the HP phase at this pressure gives a value of circa 64%. This phase transition would imply a volume collapse of approx. 1.2 %. The compression of the high-pressure $P2_12_12_1$ phase seems to be also highly anisotropic. In particular, the *b* axis is quite incompressible with only a variation of 1% between 27.4 and 45.9 GPa, whereas the *a* and *c* axes decrease 4.6 and 3.2%, respectively. Rough parameters of the tentative experimental EOS are collected in Table II and show that the high-pressure phase would exhibit a similar compressibility that the initial barite-type phase and very different from that estimated by Huang *et al.*[9] for the HP phase using the tentative $P2_1/m$ unit cell (B_0 = 117 GPa and B_0' = 3). The similarity of the bulk moduli can be explained by the fact that, in both structures, the coordination sphere of the Ba and Cr

atoms ([BaO_{12}] dodecahedra and [CrO_4] tetrahedra) would not change significantly at the transition. It is also important to remark that, as can be seen in Fig. 2, the phase transition is reversible; *i.e.* the initial barite-type structure is fully recovered after decompression.

These experimental observations are supported by *ab initio* total-energy calculations. According with calculations the barite structure is the thermodynamically stable phase at ambient pressure. As can be seen in Table I, the calculated lattice parameters and fractional coordinates compare very well to those from our experiment and previous reported data[36, 37], the unit-cell volume being only slightly underestimated (<1%). In Figure 5, it can be clearly seen that the theoretical energy-volume curves of the initial barite-type and the HP $P2_12_12_1$ post-barite-type phases cross each other at high pressure. As shown in the enthalpy difference as a function of pressure plot (Fig. 5 inset), the HP phase becomes more stable than the barite-type phase at 14.9 GPa. According to the calculations, this transformation entails a volume change of 2.2%, which is in relatively good agreement with the experimental results. The calculated fractional coordinates of this HP phase are in good agreement with those of the experimental post-barite structure reported for HP-$BaSO_4$ (see Table I and Ref. [11]). The calculated EOS parameters collected in Table II also agree well with those estimated experimentally, as can be also deduced looking at the theoretical and experimental evolution of the lattice volumes with pressure in Figure 3a. It is also important to mention that the small discontinuity in the evolution of the lattice parameters with pressure observed experimentally between 16.5 and 19.4 GPa was not reproduced by the calculations, where the unit-cell axes decrease smoothly. The nature of this anomalous behavior is not understood yet.

Figure 5 also shows the calculated total-energy for a potential post-barite $P2_1/m$ structure, similar to that theoretically predicted by Errandonea and coworkers for $AgClO_4$[13]. As can be seen in the figure, this potential candidate has been found to be energetically non-competitive for $BaCrO_4$ in the whole pressure range.

From our calculations we have also obtained the elastic constants of $BaCrO_4$. Let us now concentrate on them. For an orthorhombic material there are nine independent elastic constants, C_{11}, C_{22}, C_{33}, C_{44}, C_{55}, C_{66}, C_{12}, C_{13}, and C_{23}. The nine computed elastic constants at equilibrium pressure for the barite-type $BaCrO_4$ structure are collected in Table III, where they are compared with previous theoretical and experimental results on $BaCrO_4$[43] and $BaSO_4$[44], respectively. As can be seen, the calculated values are in rough agreement and are very close to those experimentally

observed in the isostructural $BaSO_4$ compound. The requirements for the Born mechanical stability in orthorhombic structure, *i.e.*

$C_{11} > 0, C_{22} > 0, C_{33} > 0$

$C_{44} > 0, C_{55} > 0, C_{66} > 0$

$(C_{11}+C_{22}-2C_{12}) > 0, (C_{11}+C_{33}-2C_{13}) > 0$

$(C_{11}+C_{22}+C_{33}+2C_{12}+2C_{13}+2C_{23}) > 0$

$(C_{22}+C_{33}-2C_{23}) > 0$

are fulfilled by our set of elastic constants, pointing out the mechanical stability of the barite $BaCrO_4$ at equilibrium pressure.

According the Voigt approximation[45], there is a simple relation between the isotropic bulk modulus B_V and the elastic constants C_{ij}. The computed elastic modulus $B_V = [C_{11}+C_{22}+C_{33}+2(C_{12}+C_{23}+C_{13})]/9$ is 50.4 GPa and, therefore, consistent with our result from total-energy calculations.

For completeness, we have also calculated three important parameters for further discussion on elasticity. These are the isotropic shear modulus (G), the Young's modulus (E) and the Poisson's ratio (υ). The first one is defined as the ratio between stress and strain and is used to provide a measure of the stiffness of a solid. The second one quantifies the stability of the crystal against shear. From the calculated elastic constants in the Voigt method, we can obtain:

$G_V=1/15\ [C_{11} + C_{22} + C_{33} + 3\ (C_{44} + C_{55} + C_{66}) - (C_{12} + C_{13} + C_{23})] = 24.6$ GPa

Reuss[46] also suggest a linear relation between the elastic compliance coefficients S_{ij} and the isotropic bulk B_R and the shear G_R moduli.

$B_R = 1/[S_{11} + S_{22} + S_{33} + 2\ (S_{12} + S_{13} + S_{23})] = 48.6$ GPa

$G_R = 15 / [4\ (S_{11} + S_{12} + S_{33}) - 4\ (S_{12} + S_{13} + S_{23}) + 3\ (S_{44} + S_{55} + S_{66})] = 15.02$ GPa

However, Hill[47] proved that the Voigt and Reuss equations represent upper and lower limits of the true values. He showed that the bulk modulus B and the shear modulus G can be obtained by the arithmetic mean value: $B_H = B = (B_R + B_V)/2$ and $G_H = G = (G_R + G_V)/2$.

The Young's modulus E and the Poisson ratio υ, can be calculated from the following equations:

$E_H= (9B_H\ G_H)/(G_H+3B_H)$

$\upsilon_H = ½\ [(B_H - (2/3)\ G_H)/(B_H+(1/3)\ G_H] = (3B_H - 2G_H)/[2(3B_H+G_H)]$

From our calculated elastic constants we obtain a bulk modulus $B_H = 49.5$ GPa, a isotropic shear modulus $G_H = 19.81$ GPa, a Young modulus $E_H = 52.43$ GPa, and a

Poisson's ratio υ_H of 0.32. Since the Poisson's ratio $\upsilon = 0.25$ is the lower limit for central force solids and 0.5 is the upper limit, our value indicates that the interatomic forces in this compound are mainly central. Moreover, it should be recall that the bulk modulus B represents the resistance to fracture, while the shear modulus G represents the resistance to plastic deformation. Thus, if $G/B < 0.5$ the material is considered to behave in a ductile manner, otherwise the materials behave in a brittle manner. Our value of $(G/B)_H = 0.4$ indicates that the crystal is ductile.

The behaviour of lattice vibrations under pressure may provide useful information regarding structural instabilities. In this regard, we also report the Raman, Infrared, and silent mode phonons at equilibrium pressure and their pressure derivatives for $BaCrO_4$-Hashemite[48-50]. According to group-theory analysis, the barite-type $BaCrO_4$ structure displays 36 Raman-active modes corresponding to the following decomposition at the Γ point: $\Gamma = 11A_g + 7B_{1g} + 11B_{2g} + 7B_{3g}$, while the infrared-active modes are 29: $11B_{1u} + 7B_{2u} + 11B_{3u}$. There are also seven silent modes (see Ref. 50). The Raman modes and their pressure derivatives are in good agreement with the experimental available data[9,51]. No experimental results are available to our knowledge for the infrared and silent modes of the Hashemite $BaCrO_4$. Finally, we report the Raman and Infrared modes of the $BaCrO_4$-$P2_12_12_1$ phase at 16 GPa, and the pressure derivatives[52]. According to group-theory analysis, the Raman- and IR-active modes of the post-barite phase lead to 72 ($\Gamma = 18A + 18B_1 + 18B_2 + 18B_3$) and 54 ($18B_1 + 18B_2 + 18B_3$) modes respectively at the zone-center, which mean a considerable increase in the number of different lattice vibrations. We hope that this work will stimulate future experiments in this field to cover this lacuna.

In the low-pressure barite-type structure, the sequence of Raman modes resembles very much that of other barite-type oxides. In our case, calculations show that Raman modes for frequencies smaller than 175 cm^{-1} are basically ascribed to the motion of the Ba cation and tetrahedral CrO_4 units. The internal vibrations of the CrO_4 tetrahedron spanned the frequency range from 341 to 974 cm^{-1} but with a gap between 425 and 905 cm^{-1}. The modes located between 905 and 975 cm^{-1} can be associated with the v_1 and v_3 bands of barite. For this structure, the modes with larger pressure coefficients are located between 145 and 175 cm^{-1}. The mode distribution of IR modes is similar to that of Raman, being those with the highest pressure coefficient located from 125 to 190 cm^{-1}. In contrast with Raman modes, there is a soft-mode among the IR ones: The B_{1u} mode at 329.18 cm^{-1}.

We have also calculated the Raman and IR modes for the high-pressure phase. Note that the B_1, B_2, and B_3 modes are active for both types of spectroscopy, while the A modes are only Raman active. The increase of the number of vibrations is related to the decrease of the symmetry of the structure induced by the transition. However, still there are many similitudes between the Raman and IR spectra of both phases. In particular, in the HP phase there is also a large phonon gap. In this case the gap goes from 452 to 933 cm^{-1}. The high-frequency modes are associated to internal bending and stretching vibrations of the CrO_4 tetrahedra. In the high-pressure phase, the pressure coefficients are slightly smaller than in the low-pressure phase, but differences are small, which is consistent with the fact that both phases have a similar bulk modulus. In particular, the B_1 mode calculated to be at 281.2 cm^{-1} (at 16 GPa) is the one with the highest pressure coefficient ($d\omega/dP$ = 4.49 cm^{-1}/GPa). A noticeable fact is the presence of two soft modes at 320 and 354 cm^{-1} (see Ref. 52), which suggest that upon further compression the $P2_12_12_1$ phase will become mechanically unstable. The occurrence of a second transition induced by pressure will be the focus of future studies.

In conclusion, the phase transition recently reported for $BaCrO_4$ at high-pressures is confirmed. Both, X-ray diffraction experiments and *ab initio* total-energy calculations suggest that the high-pressure phase adopts the $P2_12_12_1$ postbarite phase[11], which is basically a strong distortion of the initial barite phase. The first coordination sphere of the Ba and Cr atoms would not change and only the coordination number of the second sphere would increase from 7 to 8. This transition involves a contraction of the *a* and *c* axes of approximately 20% and 3%, respectively, and an expansion of the *b* axis of approximately 26%. This drastic change in the lattice constants is likely caused by a small displacement and a tilting movement of the [CrO_4] tetrahedra, as it occurs in $BaSO_4$[11]. Furthermore, we have found that the onset of the phase transition is highly dependent on the hydrostaticity of the pressure media. Thus, the less hydrostatic the medium is, the lower the transition pressure. This new example of postbarite-type structure confirms the location of this structural archetype in the north-east part of the barite-type compounds in the Bastide's diagram. The equations of state of both phases have been determined. We also report the *ab initio* elastic constants for the Hashemite phase, showing that the Born stability criteria are fulfilled. Finally we also obtain the Raman, Infrared, silent modes and they pressure derivatives of the low- and high-pressure phases. For both phases all modes are assigned and the most distinctive vibrations described. In particular, for the barite-type phase the agreement with previous

experiments is good being several unmeasured modes calculated, which could be an important help for future studies. All Raman and IR modes for the HP phase are also calculated. In this phase we found two soft modes, which suggest that the $P2_12_12_1$ phase will become unstable at pressures higher that those covered by this study.

Acknowledgments

Financial support from the Spanish Consolider Ingenio 2010 Program (Project No. CDS2007-00045) is acknowledged. The work was also supported by Spanish MICCIN under the projects: CTQ2009-14596-C02-01 and MAT2010-21270-C04-01/03 as well as from Comunidad de Madrid and European Social Fund: S2009/PPQ-1551 4161893 (QUIMAPRES). A. M and P. R-H acknowledge the computer time provided by the Red Española de Supercomputación (RES)

References

1 A. E. Rubin, Meteorit. Planet. Sci. **32**, 231 (1997).
2 A. Brenier, G. Jia, and C. Tu, J. Phys.: Condens. Matter **16**, 9103 (2002).
3 M. Kobayashi, M. Ishi, Y. Usuki, and H. Yahagi, Nucl. Instrum. Methods Phys. Res. A **333**, 429 (1993).
4 M. Nikl, et al., Journal of Applied Physics **91**, 5041 (2002).
5 M. O'Keeffe and B. G. Hyde, Structure and Bonding **61**, 77 (1985).
6 D. Santamaria-Perez and R. Chulia-Jordan, High Pressure Res. **32**, 81 (2012).
7 A. Vegas, Crystallography Reviews **7**, 189 (2000).
8 W. A. Crichton, M. Merlini, M. Hanfland, and H. Muller, Am. Miner. **96**, 364 (2011).
9 T. Huang, S. R. Shieh, A. Akhmetov, X. Liu, C. M. Lin, and J. S. Lee, Phys. Rev. B **81**, 214117 (2010).
10 P. L. Lee, E. Huang, and S. C. Yu, High Press. Res. **23**, 439 (2003).
11 D. Santamaria-Perez, L. Gracia, G. Garbarino, A. Beltran, R. Chulia-Jordan, O. Gomis, D. Errandonea, Ch. Ferrer-Roca, D. Martinez-Garcia, and A. Segura, Phys. Rev. B **84**, 054102 (2011).
12 P. W. Bridgman, Proc. Amer. Acad. Sci. **72**, 207 (1937).
13 D. Errandonea, L. Gracia, A. Beltran, A. Vegas, and Y. Meng, Phys. Rev. B **84**, 064103 (2011).
14 D. Errandonea and F. J. Manjon, Prog. Mater. Sci. **53**, 711 (2008).
15 R. Lacomba-Perales, D. Errandonea, Y. Meng, and M. Bettinelli, Phys. Rev. B **81**, 064113 (2010).
16 W. A. Crichton, J. B. Parise, S. M. Antao, and A. Grzechnik, Am. Miner. **90**, 22 (2005).
17 L. Gracia, A. Beltran, D. Errandonea, and J. Andres, Inorg. Chem. **51**, 1751 (2012).
18 A. P. Hammersley, S. O. Svensson, M. Hanfland, A. N. Fitch, and D. Hausermann, High Press. Res. **14**, 235 (1996).

[19] H. K. Mao, J. Xu, and P. M. Bell, Journal of Geophysical Research-Solid Earth and Planets **91**, 4673 (1986).
[20] J. Rodriguez-Carvajal, Physica B **192**, 55 (1993).
[21] G. Nolze and W. Kraus, Powder Diffr. **13**, 256 (1998).
[22] P. Hohenberg and W. Kohn, Phys. Rev. B **136**, B864 (1964).
[23] G. Kresse and J. Furthmuller, Comput. Mater. Sci. **6**, 15 (1996).
[24] G. Kresse and J. Furthmuller, Phys. Rev. B **54**, 11169 (1996).
[25] G. Kresse and J. Hafner, Phys. Rev. B **47**, 558 (1993).
[26] G. Kresse and J. Hafner, Phys. Rev. B **49**, 14251 (1994).
[27] P. E. Blochl, Phys. Rev. B **50**, 17953 (1994).
[28] G. Kresse and D. Joubert, Phys. Rev. B **59**, 1758 (1999).
[29] J. P. Perdew, A. Ruzsinszky, G. I. Csonka, O. A. Vydrov, G. E. Scuseria, L. A. Constantin, X. L. Zhou, and K. Burke, Phys. Rev. Lett. **100**, 136406 (2008).
[30] A. Mujica, A. Rubio, A. Munoz, and R. J. Needs, Rev. Mod. Phys. **75**, 863 (2003).
[31] N. Chetty, A. Munoz, and R. M. Martin, Phys. Rev. B **40**, 11934 (1989).
[32] S. Baroni, S. de Gironcoli, A. Dal Corso, and P. Giannozzi, Rev. Mod. Phys. **73**, 515 (2001).
[33] K. Parlinski, Z.Q. Li and Y. Kawazoe, Phys. Rev. Lett. **78**, 4063 (1997); K. Parlinski, Computer code PHONON, Cracow, 2008.
[34] O. Beckstein, J. E. Klepeis, G. L. W. Hart, and O. Pankratov, Phys. Rev. B **63**, 134112 (2001).
[35] J. F. Nye, *Physical properties of crystals. Their representation by tensor and matrices.* (Oxford University Press, 1957).
[36] E. N. Duesler and E. E. Foord, Am. Miner. **71**, 1217 (1986).
[37] A. Lentz, W. Buchele, and H. Schollhorn, Cryst. Res. Technol. **21**, 827 (1986).
[38] D. Errandonea, Y. Meng, M. Somayazulu, and D. Hausermann, Physica B-Condensed Matter **355**, 116 (2005).
[39] J. Ruiz-Fuertes, D. Errandonea, R. Lacomba-Perales, A. Segura, J. Gonzalez, F. Rodriguez, F.J. Manjon, S. Ray, P. Rodriguez-Hernandez, A. Muñoz, Z. Zhu, and C.Y. Tu, Phys. Rev. B **81**, 224115 (2010).
[40] E. Bandiello, D. Errandonea, D. Martinez-Garcia, D. Santamaria-Perez, and F. J. Manjon, Phys. Rev. B **85**, 024108 (2012).
[41] Y. W. Long, L. X. Yang, S. J. You, Y. Yu, R. C. Yu, C. Q. Jin, and J. Liu, J. Phys.-Condes. Matter **18**, 2421 (2006).
[42] D. Errandonea, R. S. Kumar, S. N. Achary, and A. K. Tyagi, Phys. Rev. B **84**, 224121 (2011).
[43] U. Becker, P. Risthaus, F. Brandt, and D. Bosbach, Chem. Geol. **225**, 244 (2006).
[44] C. Schaefer, L. Bergmann, E. Fues, and H. Ludloff, Sitzber. Preuss. Akad. Wiss. Phys.-Math. Kl. **1935**, 222 (1935).
[45] W. Voigt, *Lehrbuch der Kristallphysik* (Verlag und Druck, Leipzig und Berlin, 1928).
[46] Z. Reuss, Angew. Math. Mech. **9**, 49 (1929).
[47] R. Hill, Proceedings of the Physical Society of London Section A **65**, 349 (1952).
[48] See Supplemental Material at [URL will be inserted by publisher] for Raman mode phonons at equilibrium pressure of $BaCrO_4$-Hashemite and their pressure derivatives.

[49] See Supplemental Material at [URL will be inserted by publisher] for Infrared mode phonons at equilibrium pressure of $BaCrO_4$-Hashemite and their pressure derivatives.

[50] See Supplemental Material at [URL will be inserted by publisher] for silent mode phonons at equilibrium pressure of $BaCrO_4$-Hashemite and their pressure derivatives.

[51] D. Wallace and H. Callen, *Thermodynamics of crystals* (Dover, New York, 1998).

[52] See Supplemental Material at [URL will be inserted by publisher] for Raman and Infrared modes of the $BaCrO_4$-$P2_12_12_1$ phase at 16 GPa, and the pressure derivatives.

Table I.- Experimental and calculated GGA lattice parameters, volumes, and fractional coordinates of room-pressure *Pnma* barite-type phase and the high-pressure $P2_12_12_1$ post-barite-type phase. The experimental lattice parameters of the barite-type phase correspond to the indexation of our XRD pattern, but the atomic coordinates are those reported in Ref. [37]

		RP barite-type *Pnma* phase		HP post-barite-type $P2_12_12_1$ phase	
		Experimental	Theoretical	Experimental (27.4 GPa)	Theoretical (27.9 GPa)
a (Å)		9.1165(6)	9.0889	6.860(1)	6.7839
b (Å)		5.5264(4)	5.5021	6.1602(8)	6.1676
c (Å)		7.3347(5)	7.3188	6.5351(8)	6.4965
V (Å^3)		369.5(1)	366.0	276.2(4)	271.8
Ba	x	0.1830	0.1837	--	0.6356
	y	0.25	0.25		0.3022
	z	0.1553	0.1547		0.5767
Cr	x	0.5574	0.5572	--	0.6369
	y	0.25	0.25		0.2273
	z	0.8057	0.8051		0.0772
O_1	x	0.3900	0.3876	--	0.4573
	y	0.25	0.25		0.1348
	z	0.8837	0.8827		0.2179
O_2	x	0.6792	0.6812	--	0.8331
	y	0.25	0.25		0.2987
	z	0.9676	0.9689		0.2094
O_3	x	0.5847	0.5819	--	0.4322
	y	0.0113	0.0060		0.9492
	z	0.6777	0.6757		0.5366
O_4	x	--	--	--	0.6975
	y				0.0443
	z				0.9055

Table II.- Experimental, theoretical (from EOS) and previously reported unit-cell volumes at zero pressure (V_0), bulk moduli (B_0) and the first derivatives with pressure (B'_0) of both, the low-pressure barite-type and the high-pressure post-barite-type phases. Transition pressures are also indicated. In the HP phase (only 5 data points), the B'_0 value was fixed to 4.5 to avoid physically meaningless results.

EOS		**Transition pressure (GPa)**	**V_0 (Å^3)**	**B_0 (GPa)**	**B'_0**
Low-pressure barite-type phase (S.G. *Pnma*)	Experimental (This work)	~ 15	369.5(1)	53.3(9)	4.6(2)
	Theoretical (This work)	14.9	365.7(3)	56.0(8)	4.3(1)
	Experimental (Ref.[9])	9.8	369.9(2)	53(1)	6.8(5)
	Theoretical (Ref.[43])	--	370.6	56.05	--
High-pressure postbarite-type phase (S.G. $P2_12_12_1$)	Experimental (This work)	--	365(8)	53(6)	4.5 (fixed)
	Theoretical (This work)	--	370(2) 355(1)	36(2) 57(1)	6.0(2) 4.5 (fixed)

Table III.- Computed elastic constants of $BaCrO_4$-Hashemite of the present work (GPa) compared with those previously reported and with the experimental ones corresponding to $BaSO_4$.

	$BaCrO_4$ Theoretical (This work)	**$BaCrO_4$ Theoretical (Ref. [43])**	**$BaSO_4$ Experimental (Ref. [44])**
C_{11}	106.9	102.5	88.3
C_{22}	71.8	92.6	78.1
C_{33}	101.8	111.7	103.8
C_{44}	5.5	12.5	11.7
C_{55}	35.6	35.5	28
C_{66}	17.2	23.9	25.5
C_{12}	32.4	38.1	47.7
C_{13}	29.7	32.3	28.9
C_{23}	24.3	29.3	26.9

Figure captions.

Figure 1.- (a) Barite-type structure of $BaCrO_4$ at room conditions projected on to the *ac*-plane. Orange and green and tiny red circles represent Ba, Cr and O atoms, respectively. (b) Structure of the high-pressure phase of $BaCrO_4$ at 45.9 GPa projected also on the same projection.

Figure 2.- Powder x-ray diffraction patterns of $BaCrO_4$ at increasing pressure conditions using He as pressure transmitting medium. Black arrows indicate the appearance of new peaks and asterisks denote the diffraction maxima of Re (gasket material).

Figure 3.- (a) Experimental and calculated pressure dependence of the unit-cell volume for the two phases of $BaCrO_4$. Black squares (red dashed line) and blue circles (blue dashed line) correspond to the experimental (calculated) data for the barite-type and the post-barite-type phases. (b) Evolution of the lattice parameters of the LP barite-type phase with pressure. Squares, circles and triangles represent the *a*, *b* and *c* axes. Black solid and empty symbols correspond to experiments and calculations, respectively. Green symbols correspond to experimental results reported in Ref. [9]. The shadowed region indicates the small discontinuity in lattice constants.

Figure 4.- LeBail refinement of the x-ray diffraction pattern of $BaCrO_4$ at 45.9 GPa. Observed, calculated and difference profiles are represented as black, red and blue lines. Vertical markers indicate Bragg reflections of the *Pnma* barite-type (top), $P2_12_12_1$ postbarite-type (center) structures and the rhenium gasket (bottom).

Figure 5.- Internal energy as a function of volume for the *Pnma* barite-type structure, and the $P2_12_12_1$ postbarite-type structure of $BaCrO_4$. The $P2_1/m$ (S.G. 11) structure proposed by Errandonea *et al.* for a high-pressure phase of $AgClO_4$ is also included.[13] Inset: Enthalpy variation versus pressure.

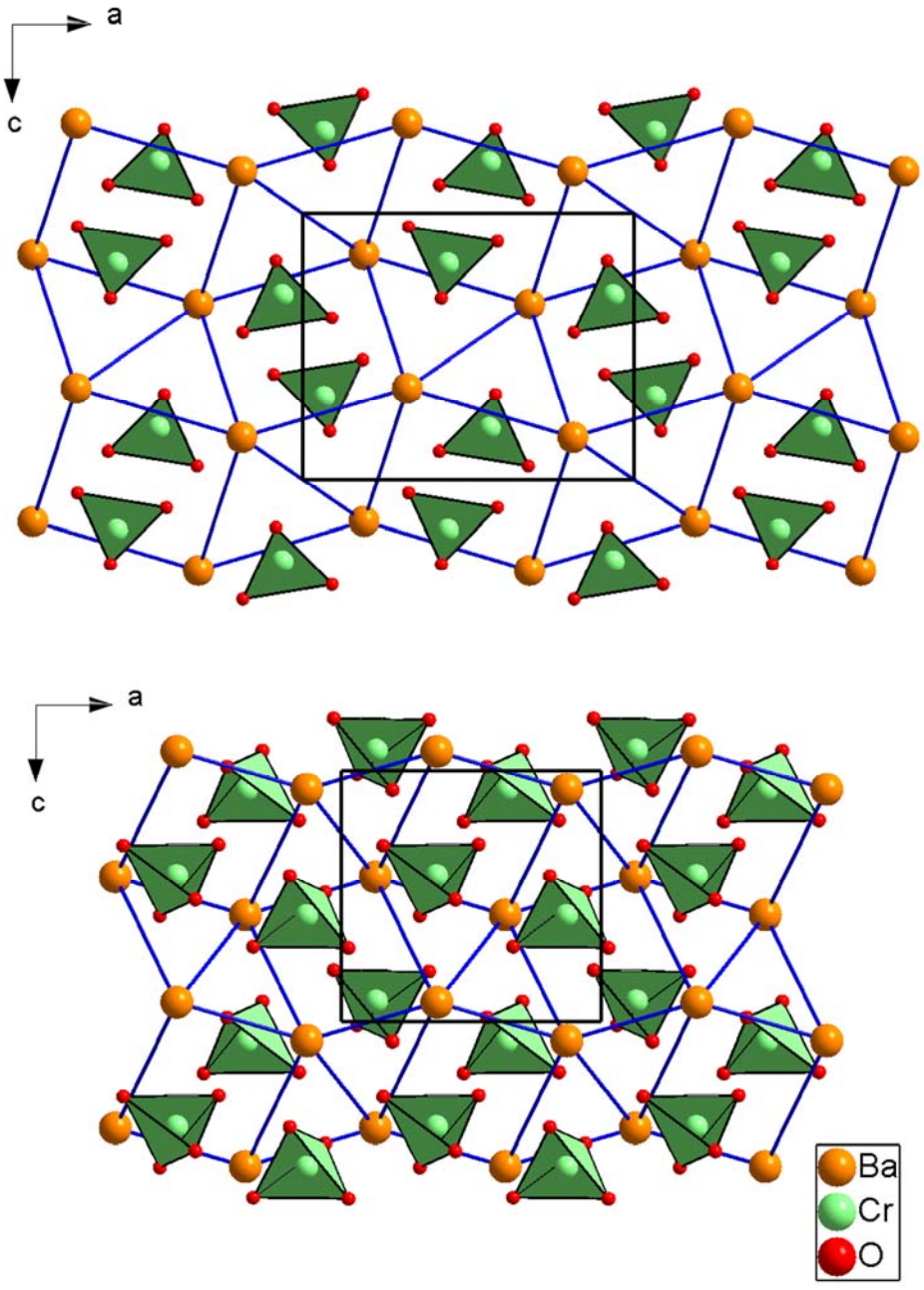

Figures 1a and 1b

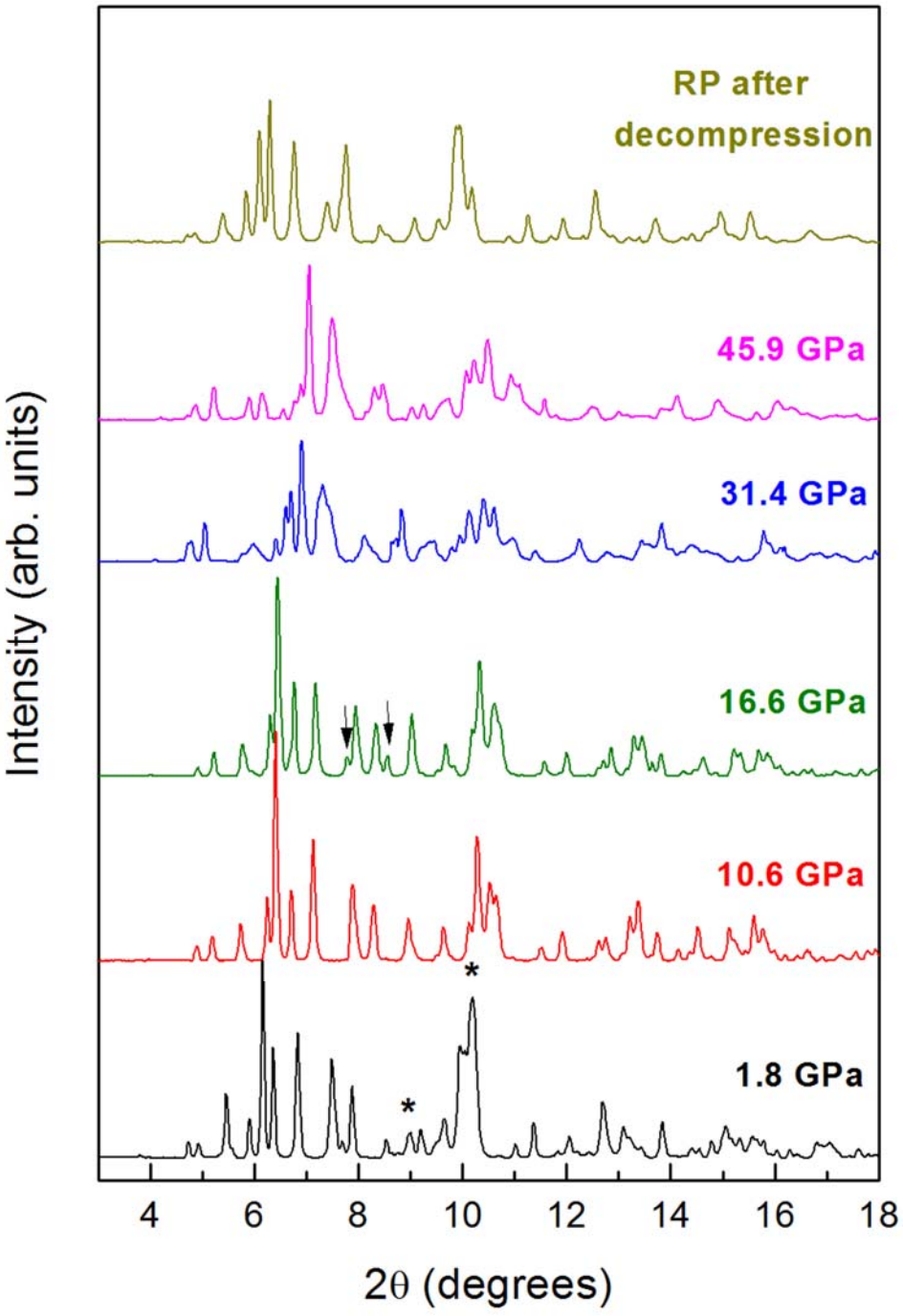
RP after
decompression
45.9 GPa
31.4 GPa
16.6 GPa
10.6 GPa
1.8 GPa
*
*
Intensity (arb. units)
4
6
8
10
12
14
16
18
2θ (degrees)

Figure 2

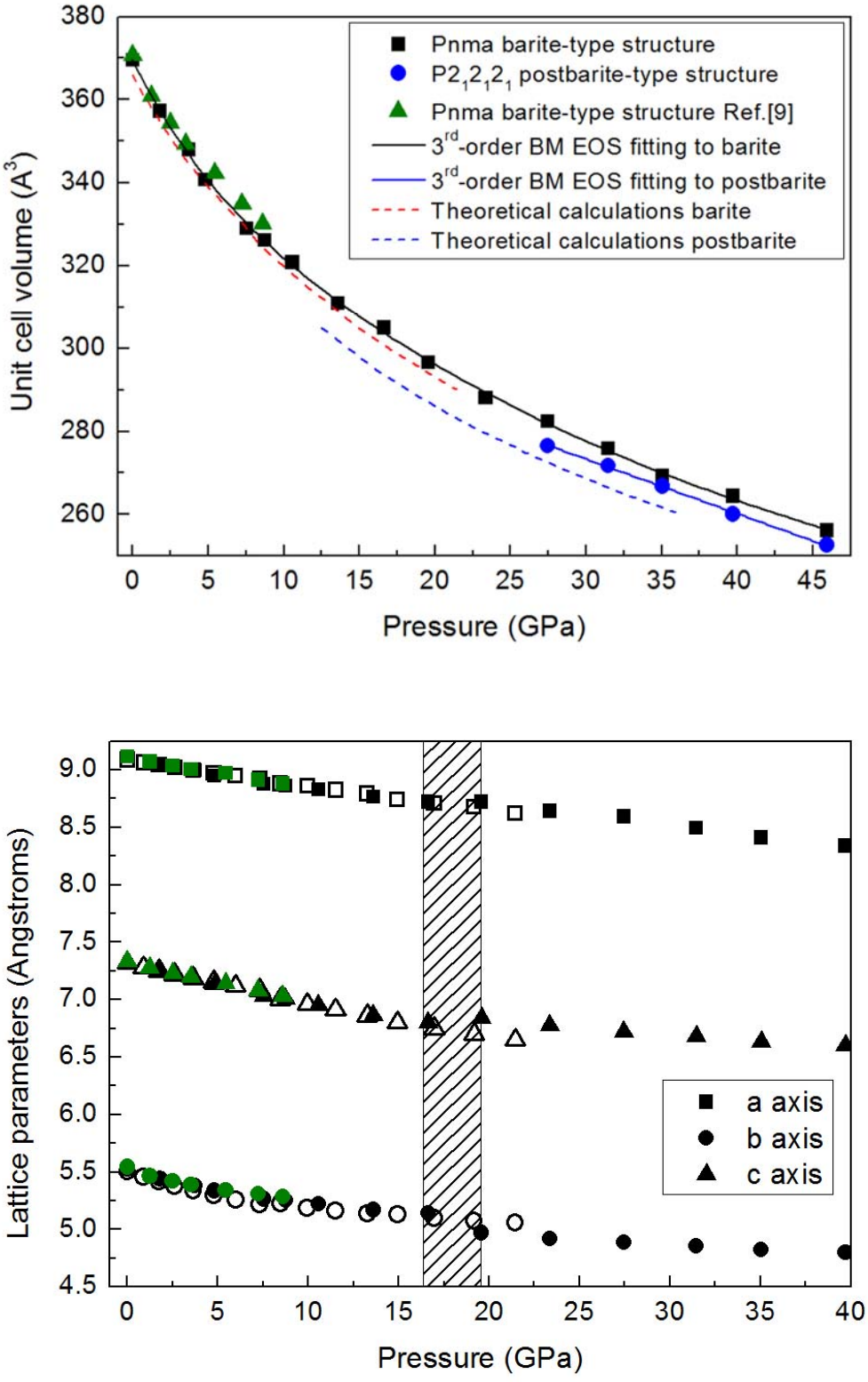

Figure 3a and 3b

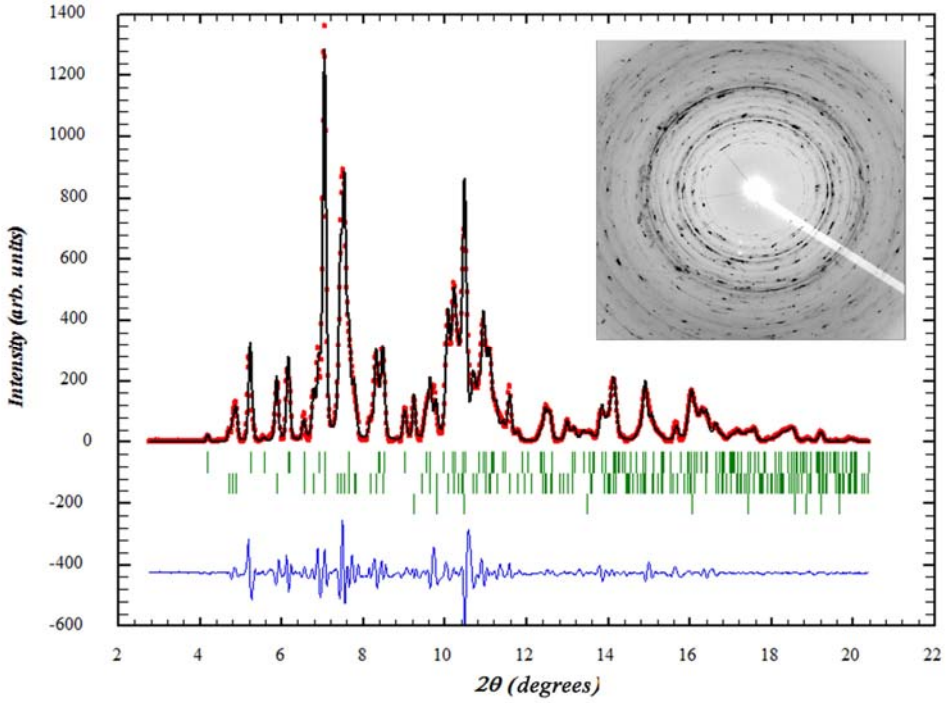
1400
1200
1000
800
600
400
200
0
-200
-400
-600
Intensity (arb. units)
2
4
6
8
10
12
14
16
18
20
22
2θ (degrees)

Figure 4

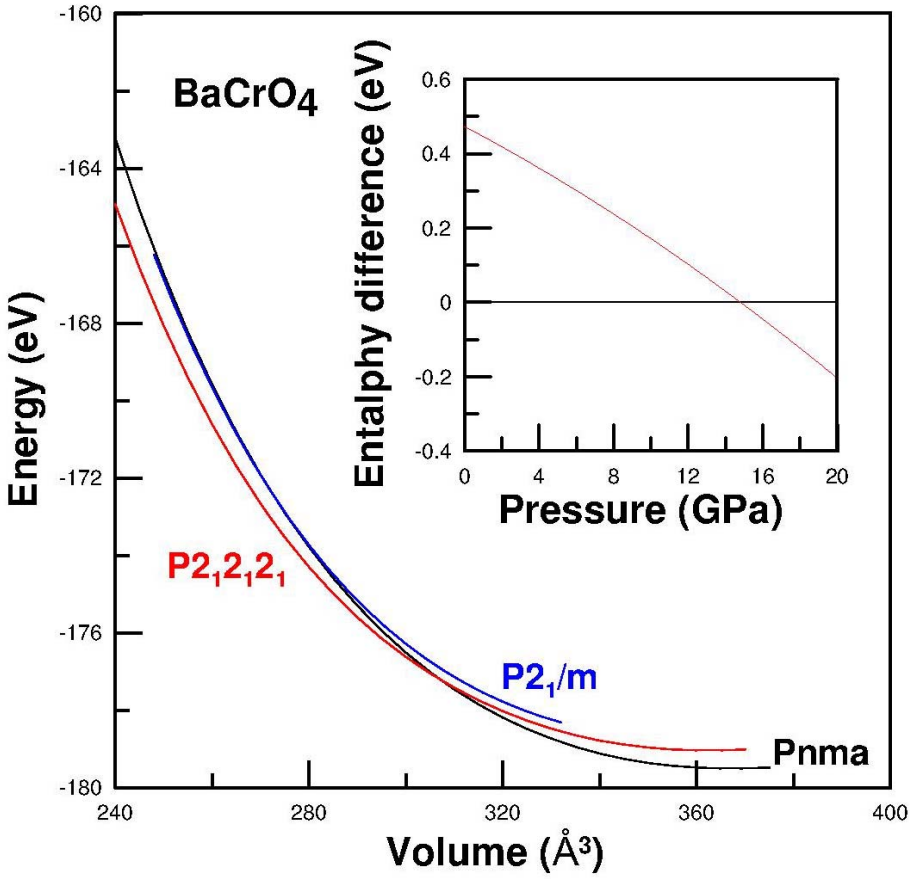
BaCrO4
Energy (eV)
Volume (Å3)
Entalphy difference (eV)
Pressure (GPa)
P21212
P21/m
Pnma
-160
-164
-168
-172
-176
-180
240
280
320
360
400
0.6
0.4
0.2
0
-0.2
-0.4
0
4
8
12
16
20

Figure 5